

# Empirical evidences for a planetary modulation of total solar irradiance and the TSI signature of the 1.09-year Earth-Jupiter conjunction cycle

Nicola Scafetta<sup>1,2</sup> and Richard C. Willson<sup>1</sup>

the date of receipt and acceptance should be inserted later

**Abstract** The time series of total solar irradiance (TSI) satellite observations since 1978 provided by ACRIM and PMOD TSI composites are studied. We find empirical evidence for planetary-induced forcing and modulation of solar activity. Power spectra and direct data pattern analysis reveal a clear signature of the 1.09-year Earth-Jupiter conjunction cycle, in particular during solar cycle 23 maximum. This appears to suggest that the Jupiter side of the Sun is slightly brighter during solar maxima. The effect is observed when the Earth crosses the Sun-Jupiter conjunction line every 1.09 years. Multiple spectral peaks are observed in the TSI records that are coherent with known planetary harmonics such as the spring, orbital and synodic periods among Mercury, Venus, Earth and Jupiter: the Mercury-Venus spring-tidal cycle (0.20 year); the Mercury orbital cycle (0.24 year); the Venus-Jupiter spring-tidal cycle (0.32 year); the Venus-Mercury synodic cycle (0.40 year); the Venus-Jupiter synodic cycle (0.65 year); and the Venus-Earth spring tidal cycle (0.80 year). Strong evidence is also found for a 0.5-year TSI cycle that could be driven by the Earth's crossing the solar equatorial plane twice a year and may indicate a latitudinal solar-luminosity asymmetry. Because both spring and synodic planetary cycles appear to be present and the amplitudes of their TSI signatures appear enhanced during sunspot cycle maxima, we conjecture that on annual and sub-annual scales both gravitational and electro-magnetic planet-sun interactions and internal non-linear feedbacks may be modulating solar activity. Gravitational tidal forces should mostly stress spring cycles while electro-magnetic forces could be linked to the solar wobbling dynamics, and would mostly stress the synodic cycles. The observed statistical coherence between the TSI records and the planetary harmonics is confirmed by three alternative tests.

**Keywords** solar dynamo · solar total irradiance · helioseismology · planet-star interactions · magnetohydrodynamics (MHD)

## 1 Introduction

Numerous observations – e.g. sunspot, total solar irradiance (TSI) satellite (Willson and Mordvinov, 2003; Fröhlich, 2006) and magnetic flux records (Ball et al., 2012) – have demonstrated that solar activity is characterized by a variable  $\sim 11$ -year Schwabe cycle, by complex dynamics on monthly-to-annual time scales and by possible multi-decadal trending. In addition to a varying 11-year solar cycle, spectral analyses of solar records have also identified a number of distinct periodicities at the multidecadal, secular and millennial scales (Abreu et al., 2012; Bond et al., 2001; Frick et al., 1997; Ogurtsov et al., 2002; Scafetta, 2012c; Scafetta and Willson, 2013; Tan, 2011). The statistically estimated periodicities depend on the length and nature of the analyzed records. However, typical major spectral peak values are found at 43-45 years, 55-61 years, 81-87 years (Gleissberg), 98-130 years, 150-180 year,  $\sim 207$  years (de Vries),  $\sim 500$  years,  $\sim 980$  years (Eddy), and others. See for example Scafetta (2012c) and Scafetta and Willson (2013) where high resolution spectral analyses of a 438-year long auroral record and of a 9,400 solar proxy model (Steinhilber et al., 2012) are proposed.

The conventional view of solar science has been that solar magnetic and radiant variability are driven by internal solar dynamics alone, characterized by hydromagnetic solar dynamo models (Tobias, 2002; Jiang et al., 2007). However, current solar dynamo models assume that the Sun is an isolated system and have been unable to explain and/or forecast solar variability including the emergence of the Schwabe 11-year cycle and of its multidecadal, secular and millennia modulations. In fact, although solar dynamo theories do predict the emergence of generic solar oscillations, the reason why, among all possible theoretical frequencies, the Sun oscillates at the specific observed frequencies and phases has eluded researchers so far. For example, periods of low solar activity such as the Maunder and Dalton minima, and the intra-annual oscillations

<sup>2</sup>Duke University, Durham, NC 27708

larger than the monthly solar differential rotation cycles are essentially not predicted by the solar dynamo models, which require an arbitrary choice of specific free parameters even for reproducing an 11-year major oscillation (Jiang et al., 2007).

An alternative theory for solar variability was first put forth in the 19th century by numerous auroral and solar specialists such as Wolf (1859), and investigated later by Brown (1900), Luby (1948) and others. It proposes that solar magnetic and radiant variability is partially regulated by planetary gravitational and magnetic forcings. This theory was originally suggested by the related facts that: (1) sunspot activity was found to be characterized by an  $\sim 11$ -year cycle; and (2) the Schwabe frequency band falls between the two primary tidal cycles associated with the Jupiter-Saturn spring tide (9.93-year) and with Jupiter's orbital period (11.86-year). Bendandi (1931) observed that the tides of Venus, Earth and Jupiter generate a recurrent oscillation at the period of 11.07 years and Wood and Wood (1965) observed that the solar-jerk function presents a period of 11.08 years. Indeed, the average 11-year solar cycle length is 11.05-11.10 years (Scafetta, 2012c). These results have been more recently confirmed and expanded (e.g.: Hung, 2007; Scafetta, 2012c,d). Thus, internal solar dynamo mechanisms may be synchronized to the frequencies of the external planetary harmonic forcings.

The planetary theory of solar variation has not found support within the mainstream solar physics community during the last decades because: (1) it was found problematic to qualitatively relate secular solar variability to planetary cycles (Smythe and Eddy, 1977); (2) planetary forcings appear weak over the sun-planet distances (Callebaut et al., 2012); (3) although planetary induced solar luminosity enhancement observations have been reported for numerous extrasolar planets (Scharf, 2010; Gurdemir et al., 2012; Wright et al., 2008) interpretation of the data referring to distant solar systems remains controversial (Poppenhaeager and Schmitt, 2011). While some cyclical variability has been observed in numerous sun-like stars (Baliunas et al., 1995) unambiguous planetary influence cannot be deduced since the planetary configuration of those distant solar systems is mostly unknown, stellar data are available only for a few decades at most and their quality may be still too poor.

The planetary configuration of our solar system is known very well and there are solar data and magnetic activity proxy models spanning decades to millennia that are of relatively high quality. A number of empirical studies have found preliminary evidence for planetary influences on solar behavior (Bigg, 1967; Charvátová and Štěpáček, 1991; Cionco and Compagnucci, 2012; Fairbridge and Shirley, 1987; Hung, 2007; Jose, 1965; Juckett, 2000, 2003; Landscheidt, 1999; Leal-Silva and Velasco Herrera, 2012; Sharp, 2013; Wilson et al., 2008). Spectral analysis has recently revealed that the sunspot Schwabe cycle may be made and modulated by at least three frequencies (Scafetta, 2012c): the two Jupiter and Saturn tidal cycles (9.93 and 11.86 year) and the strong central 10.87-year dynamo cycle, which may also emerge from other planetary recurrent cycles varying between 10.40 and 11.10 years due to Venus, Earth and Jupiter. A harmonic model based on these three major frequencies suffices to hindcast the major solar secular solar oscillation (e.g. the Oort, Wolf, Spörer, Maunder and Dalton minima) and the millennial solar oscillation as interference patterns produced by the three cycles throughout the Holocene. Thus, if planetary harmonics are synchronizing and modulating the solar dynamo, specific major oscillations (quasi 11-year, 20-year, 42-45-year, 61-year, 86-year, 115-year, 130-year, 170-180-year, 207-year, 500-year and 1000-year cycles) would characterize solar activity. Indeed, these oscillations are commonly observed in both solar and the Earth's climate records (Bond et al., 2001; Ogurtsov et al., 2002; Qian and Lu, 2010; Chylek et al., 2012; Steinhilber et al., 2012; Scafetta, 2012c,d). Other recent studies have noted planetary harmonics in the sunspot record, auroral records, microwave emission and multi-millenia cosmo-nucleotide proxy solar models (Abreu et al., 2012; Scafetta, 2012a; Scafetta and Willson, 2013; Tan and Cheng, 2012).

The physical problem is not solved yet and is highly controversial. However, preliminary gravitational physical mechanisms have been recently proposed (Wolff and Patrone, 2010; Scafetta, 2012d; Abreu et al., 2012). Internal solar feedback processes could also lead to increased magneto-acoustic heating, dynamo action and direct magnetic interactions between stellar and planetary magnetic fields (e.g: Cuntz et al., 2000; Scharf, 2010). Alternative physical mechanisms may also simultaneously act and/or be complementary to each other. For example, gravitational tides and electromagnetic mechanisms may generate alternative sets of harmonics with the former stressing the spring harmonics and the latter the synodic harmonics among the planets.

Wolff and Patrone (2010) argued that planetary gravitational forcing could cause a mass flow inside the Sun that could carry fresh hydrogen fuel to deeper levels including the solar core consequently increasing the solar nuclear fusion rate. Abreu et al. (2012) proposed that planetary tides could exert a varying torque on a non-spherical tachocline, perturb the operation of the solar dynamo and modulate the long-term solar magnetic activity. Abreu et al. (2012) found that the torque signal presents numerous harmonics on the secular and multisecular scales in common with long solar proxy models. In general, a frequency matching between solar and planetary harmonics may be achieved adopting alternative physical functions of the orbits of the planets and, therefore, it would suggest the existence of a physical link between planetary orbits and solar activity, without necessarily specifying the exact physical mechanisms involved in the process.

Scafetta (2012d) observed that planetary gravitational tidal forcing alone appears too weak to directly force the solar tachocline or the solar convection zone. Callebaut et al. (2012) dismissed a possible direct planetary forcing of the solar convection zone by arguing that the internal convection velocities and accelerations are far greater than those derivable from

planetary tidal influences. The claim needs to be partially reconsidered because Shravan et al. (2012) have recently found that the solar convection velocities appear to be 20-100 times weaker than the previous theoretical estimations. Scafetta et al. (2013) have shown other shortcomings of the Callebaut et al. analysis. In any case, it appears that planetary forcings may modulate solar activity only if internal solar mechanisms greatly amplify their effects.

Scafetta (2012d) proposed that the gravitational energy released by the planetary tides to the sun may trigger slight nuclear fusion rate variations by enhancing solar plasma mixing. In fact, solar plasma is made of protons and electrons that can freely move and interact through electromagnetic forces. Under gravitational perturbations electrons and protons may drift in opposite directions perpendicular to the gravitational forces generating micro currents in the plasma. For example, in a magnetic field  $\mathbf{B}$  a plasma moved by a local gravitational field  $\mathbf{g}$  has its protons and electrons drifting with a velocity given by  $\mathbf{v}_g = m\mathbf{g} \times \mathbf{B}/qB^2$ , where the dependence on the charge  $q$  of the particle implies that the drift direction is opposite for protons and electrons, resulting in an electric current. This relative movement of electrons and protons may cause a local reduction of the electric repulsion among protons, which can enhance and modulate the nuclear fusion rate in proportion to the strength of the gravitational tides acting in the core. A nuclear fusion enhancement can yield a significant amplification of the gravitational tidal energetic signal released to the sun.

Scafetta (2012d) observed that a gravitational triggering of the nuclear fusion rate could be possible because main-sequence stars are characterized by a delicate balance between nuclear fusion activity and gravitational forces. Essentially, in stars gravity triggers nuclear fusion activity and controls it, and every gravitational variation inside the star could trigger a variation of the luminosity production. Scafetta proposed a physical theory to quantify the phenomenon based on the stellar mass-luminosity relation:  $L_1/L_2 \sim (M_1/M_2)^4$  (Duric, 2004). The stellar mass-luminosity relation may also be interpreted as a relation between a star's luminosity and the gravitational work released to the star by solar gravitational forces, which are related to the solar mass. For example, if the mass of the planets of the solar system were added to the Sun, the solar luminosity should increase by about 0.5%, and TSI would increase by about  $7.4 \text{ W/m}^2$ .

The nuclear fusion amplification mechanism proposed by Scafetta (2012d) causes an amplification of the tidal signal through nuclear fusion enhancement of the order of  $A \approx 4 \cdot 10^6$ , which can produce a small tidal-induced luminosity variation comparable with that of the observed TSI fluctuations, that is up to  $0.05\text{-}1 \text{ W/m}^2$  (Willson et al., 1986; Willson and Hudson, 1991; Willson and Mordvinov, 2003). If Scafetta's proposal is correct, a tidal induced luminosity signal may be sufficiently strong to synchronize the operation of the solar dynamo. For example, it would produce a sufficiently strong planetary tidal induced solar bulge on a  $\sim 6^\circ$  inclined plane (the solar system disk), relative to the solar equatorial bulge, causing a varying torquing force on the solar convection zone (see also Luby, 1948). Scafetta (2012d)'s theoretical model predicts the two tidal cycles ( $\sim 9.93$  years and  $\sim 11.86$  years) associated with Jupiter and Saturn observed in the sunspot record as well as significant complex intra-annual fluctuations. The complex intra-annual oscillation would be dominated by the  $\sim 0.32$ -year Jupiter/Venus spring tide oscillation and by numerous other specific planetary frequencies. Scafetta (2012d) also noted that the pattern of these fluctuations approximately repeats every 11.08 years. This period corresponds to the average Schwabe solar cycle length (Scafetta, 2012c).

In response to typical reservations expressed about gravitational triggering of the nuclear fusion rate, namely that photons diffuse very slowly from the core to the tachocline (e.g., the Kelvin–Helmholtz timescale for the Sun may be as long as  $10^4\text{-}10^5$  years) and any core luminosity fluctuation would be damped before reaching the tachocline, Wolff and Patrone (2010) and Scafetta (2012c,d) postulated the existence of fast acoustic-like or g-wave transport mechanisms. Wave mechanisms could transport an energy variation signal from the core to the tachocline within a time scale of a few weeks. Essentially, as the core luminosity production varies, the core would expand and contract in function of the strength of the planetary tides and this perturbation should be felt by the entire sun quite fast. Once at the tachocline, the small harmonic signal emerging from the radiative zone would force the convection zone, synchronize the operation of the solar dynamo and, finally, modulate the solar luminosity outputs. It may be conjectured that a gravitational planetary modulation of the solar luminosity production could be demonstrated by a synchronized variation of the solar neutrino production. However, a test of this hypothesis is not currently possible because the statistical uncertainty of neutrino measurements is too large (up to 20%-50% of the observed value) (Sturrock et al., 2006), while the magnitude of Scafetta (2012d)'s hypothesized planetary-induced luminosity variation is about 0.05%-0.005% of the solar luminosity.

A final important observation is that even if planetary forcings are modulating solar activity the magnitudes of their effects on solar observables cannot be estimated with precision because the exact physical forcing mechanisms (gravitational and electromagnetic) and internal feedbacks – e.g. resonances and synchronization mechanisms (Pikovsky et al., 2001) that may produce internal dynamical amplifications but also prevent the formation of too regular harmonics characterized by sharp spectral peaks – remain controversial and largely unknown. However, if planetary forcings are modulating solar activity, their effects should generate a complex set of harmonics associated with the periods of the planetary orbits and their mutual spring and synodic cycles. Thus, specific frequencies bands of the records describing solar activity are expected to be activated by planetary forcings. As an analogy, in the case of the ocean tides on the Earth only theoretical frequencies can be carefully calculated from astronomical considerations while the actual amplitudes and phases of the single harmonics can only be directly

measured from tide gauge records because the exact physical mechanisms generating them are not known with precision (Kelvin, 1881; Doodson, 1921; Wang et al., 2012). Therefore, a planetary modulation of solar activity can be demonstrated by studying the spectral harmonics of solar activity records and by checking whether a common set of frequencies between the solar records and the theoretical planetary frequencies exists.

Herein we conjecture that planetary harmonic signatures should be observed in total solar irradiance (TSI) satellite observations on the monthly-to-annual scales too as shown in a recent conference presentation by Scafetta (2010b). Thus, herein we study whether the ACRIM and PMOD TSI satellite composites (both continuous in TSI since 1978) present signatures of planetary harmonics.

## 2 TSI data and harmonic orbital expectations

Composites of TSI satellite observations are continuous since late 1978. The two most cited composites are the ACRIM (Willson and Mordvinov, 2003) and PMOD (Fröhlich, 2006). Before mid-1992 ACRIM and the PMOD disagree about the quality and use of the extant TSI data, and the composites disagree in important ways (Fröhlich, 2006; Scafetta and Willson, 2009; Scafetta et al., 2011). Fröhlich (2006) alters NIMBUS7/ERB and ACRIM1 published records (Willson et al., 1981; Willson and Hudson, 1991; Willson, 1997) for reasons that are disputed by the original science teams (Willson and Mordvinov, 2003; Scafetta and Willson, 2009). Because of the data controversy we will confine our spectral analysis to the less disputed ACRIM data for mid-1992 to 2012. In this range the ACRIM composite is comprised of the results from the ACRIM2 (1992-2000) and ACRIM3 (2000-2012) experiments. During this same period the PMOD composite is comprised of the ACRIM2 (1992-1996 and part of the period 1998-1999) and VIRGO results (most of 1996-2012). Since variable data patterns are amplified during solar active periods, we compare ACRIM and PMOD during the maximum of solar cycle 23 (1997.75-2004.25).

Because we are observing the Sun from satellites orbiting the Earth the major cycle found in TSI satellite raw data is related to the 1-year Earth's orbital cycle. TSI records are carefully rescaled to 1 AU using accurate ephemerides, corrected for sensor degradation and temperature sensitivities. A rigorous 1-year cycle, if found, could be due to uncorrected sensor artifacts and/or to a latitudinal solar luminosity asymmetry. If an annual cycle is found it should be carefully analyzed and accounted for, if necessary.

The strongest theoretical planetary induced tides on the Sun are produced by Jupiter, followed by Venus, Earth and Mercury, in order of magnitude and their values are calculated in Scafetta (2012d). If electro-magnetic interactions throughout the Parker heliospheric current spiral exist, Jupiter would still be the planet with the greatest effect because it has the largest magnetosphere. Earth and Venus would influence the high frequency component of the spectrum, while the other Jovian planets (Saturn, Uranus and Neptune) could more likely influence the low multidecadal and multiseccular variability (Abreu et al., 2012; Scafetta, 2012c; Scafetta and Willson, 2013; Sharp, 2013).

Herein we are looking for high frequency harmonics with period up to about 1.2 years. The gravitational tidal cycles stress the spring tides among the planets. Other mechanisms (e.g electromagnetic couplings) would be superimposed upon the tidal cycles and would stress the planetary synodic/conjunction cycles. Electromagnetic mechanisms may be related to the speed and jerk functions of the Sun relative to the barycenter of the solar system (Scafetta, 2010a, 2012d). Specific torque components acting on the solar masses could be related to the z-axis of the tidal forcings.

If TSI is modulated by planetary forces the records should be characterized by numerous planetary harmonics. The most relevant periods involve the four major tidal planets: Mercury, Venus, Earth and Jupiter (see Table 1). Table 2 lists additional spring and synodic periods using the four minor tidal planets: Mars, Saturn, Uranus and Neptune. Given the periods of two planets  $P_A$  and  $P_B$ , their synodic period  $P_{AB}$ , which is twice the spring period, is defined as

$$P_{AB} = \frac{1}{|1/P_A - 1/P_B|}. \quad (1)$$

A major cycle is anticipated for the strong Venus-Jupiter spring tidal cycle with a periodicity of  $\sim 0.32$ -year. A 0.5-year periodicity TSI harmonic could be produced by the Earth's crossing the solar equator twice a year, providing a changing view of the northern and southern solar hemispheres. If the Jupiter side of the Sun is the brightest one, the Earth-Jupiter synodic cycle should cause a TSI cycle with a  $\sim 1.092$ -year periodicity.

Table 3 lists addition relevant harmonics. These include the solar differential equatorial and polar rotation cycles relative to the fixed stars and to the four major tidal planets. We use an adaptation of Eq. 1 where one planetary harmonic is substituted with the solar rotation periods. Table 3 also lists the spring and synodic periods of Mercury, Venus and Earth relative to the synodic periods of Jupiter and Saturn, and Jupiter and Earth using the three-synodic equation:

$$P_{A(BC)} = \frac{1}{|1/P_A - |1/P_B - 1/P_C||}. \quad (2)$$

Other harmonics related to specific planetary configurations are possible, but are ignored herein.

### 3 Spectral Coherence between TSI records and planetary harmonics

Spectral analysis results are shown in Figure 1. Figure 1A depicts the traditional Lomb (unevenly sampled data: Press et al., 1997) periodogram of the 1992.5-2012.9 ACRIM TSI record. The statistical confidence of the frequency peaks is tested against red-noise background at 95% and 99% levels. Moreover, the standard deviation of the data within the analyzed frequency band (for periods less than 1.2 year),  $\sigma_d = 0.34 W/m^2$ , is 26 times larger than the average instrumental statistical error ( $\sigma_i = 0.013 W/m^2$ ). So, the observed TSI frequency patterns cannot be due to random uncertainties in the measurements.

Figure 1B uses the maximum entropy methodology (MEM: Press et al., 1997) in the traditional manner (Courtillot et al., 1977; Scafetta, 2012b) to reanalyze the ACRIM record and compare it with the PMOD record during solar cycle 23 activity maximum (1997.75-2004.25) when PMOD contains mostly non-ACRIM data. The results depicted in Figures 1A and 1B were derived using different methodologies, data and time intervals. They validate each other because a common set of statistically significant spectral peaks is found at about 0.32 year, 0.5 year and 1.09 year.

Figures 1A and 1B also depict the major frequency bands (yellow boxes) associated with theoretical planetary harmonics deduced from the spring, orbital and synodic periods among the major tidal planets (Mercury, Venus, Earth and Jupiter): see Tables 1, 2 and 3. We assume an average  $\pm 5\%$  variability in the periods which is caused by three factors. The first is the elliptical shape of planetary orbits that make spring and synodic periods vary while the theoretical orbital periods do not vary significantly (Mercury-Venus spring period varies as  $0.198 \pm 0.021$  year, Earth-Jupiter synodic period varies as  $1.092 \pm 0.009$  year, Venus-Earth spring period varies as  $0.799 \pm 0.008$  year: see Table 1). Second, there may be an internal nonlinear solar response that makes the TSI periodicities fluctuate around the theoretical forcing frequencies. Third, there are statistical errors in the data and in the power spectrum evaluations.

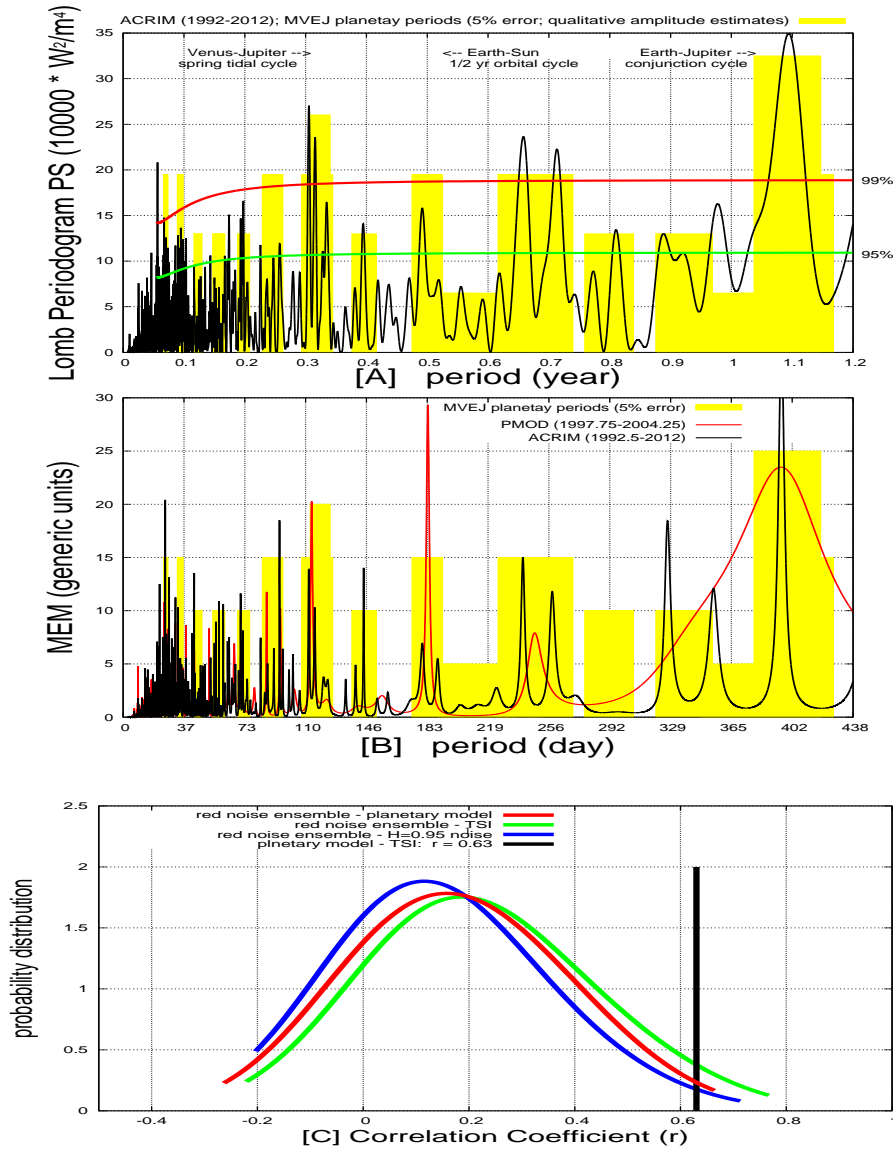
The yellow bar histogram shown in Figure 1A and 1B provides a best guess representation of the planetary spectrum constructed using bars centered on the planetary frequencies listed in the tables with a  $\pm 5\%$  width. The relative heights of the bars take into account: (1) a possible relative strength calculated using the weight  $d^{-3}$  where  $d$  is the distance a planet from the Sun (the greatest effect is given by Mercury followed by Venus, Earth and Jupiter); (2) the mass  $M$  of the planet (the greatest effect is given by Jupiter, followed by Earth, Venus and Mercury); (3) the strength of the planetary magnetosphere (the greatest effect is given by Jupiter, followed by Earth, Venus and Mercury); (4) spring and synodic oscillations should be stronger than orbital periods; and (5) symmetries associated with the Earth's orbit due to the fact that TSI is defined as the solar irradiance radiated toward the Earth at 1 astronomical unit from the Sun. Finally, analogous to Kelvin (1881)'s ocean tidal method that determines the tidal amplitudes from tide gauge records, the heights of the bars are chosen to reproduce the correspondent heights observed in the peaks of the TSI power spectrum functions. Our choice of the heights of the yellow bars should be considered best guesses due to the fact that, as explained above, it is not possible at the moment to deduce the TSI harmonic amplitudes from physical principles regulating planet-sun interactions.

Figure 1A and 1B show that major TSI spectral peaks are found within our spectral bands at 0.30-0.33 years, 0.5 years and 1.09 years that characterize major expected planetary harmonics. Other expected frequency clusters within our spectral bands at 0.2 year, 0.25 year, 0.4 year, 0.6-0.7 year and 0.9-1 year are observed. This result is particularly evident in Figure 1A where the longer TSI record from mid-1992 to 2012 is used. Thus, a simple visual analysis between the TSI spectra and the expected planetary-induced harmonics depicted in Figure 1 already suggests that planetary forcings modulate TSI. It should be noticed that a rigorous 1-year cycle is not seen in the analysis reported in the figure.

#### 3.1 Test #1: Monte Carlo red-noise simulation

Here we present two different tests to evaluate the coherence between the TSI spectrum and the planetary harmonics. The first test is depicted in Figure 1C and it is based on a Monte Carlo simulation for determining the statistical significance of the spectral correlation between the TSI periodogram and the yellow schematic planetary spectral model in Figure 1A, which represents our physical hypothesis. The found correlation value is  $r \approx 0.63$  and is indicated by a black vertical bar in Figure 1C. The test is run against the null hypothesis that the TSI record may be a red-noise signal. This test aims to determine how easy would be to find a surrogate red-noise random signal characterized by a periodogram correlated with the planetary spectrum model (indicated by the yellow histogram) with a spectral coherence correlation coefficient  $r \gtrsim 0.63$ .

We use red-noises because they are statistical autocorrelated signals generated by typical dynamical fractal mechanisms. This is how self-regulating, autocorrelated chaotic systems generally evolve and how solar activity would be expected to evolve if a specific set of harmonic forces did not regulate it. Our Monte Carlo test uses 15,000 red-noise sequences as TSI surrogate records with different Hurst exponents,  $H$ , varying between 0.85-1.05, corresponding to the range of the solar fractal variability. The average Hurst exponent for TSI has been measured to be  $H = 0.95$  (Scafetta and West, 2003; Scafetta



**Fig. 1** [A] Periodogram of ACRIM results in  $W^2/m^4$  units for data from 1992.5-2012, against red noise background at 95% and 99% confidence level (Ghil et al., 2002). [B] Power spectrum based on the Maximum Entropy Method of ACRIM (1992.5-2012.9) and PMOD during the maximum of solar cycle 23 (1997.75-2004.25). The yellow bars are a representation of the planetary spectrum due to the harmonics generated by the planets reported in Tables 1-3. [C] Monte Carlo tests to determine the statistical confidence of the correlation coefficient between the yellow area representing a spectral model of the planetary oscillations and the observed TSI periodogram of figure A ( $r \approx 0.63$ ; black).

et al., 2004; Scafetta and West, 2005). Thus, we repeated the spectral analysis using these 15,000 different red-noise records of length equal to the analyzed TSI data. The periodogram of each TSI surrogate record is calculated and cross-correlated with the yellow schematic planetary spectral curve representing our physical hypothesis by repeating the same measure used for the original TSI record. It is found that the 15,000 independent TSI synthetic records produce periodograms that correlate with the yellow planetary function with a spectral coherence correlation coefficient  $r \leq 0.66$  and only 8 red-noise simulations produced a  $r$  value larger than 0.63. The probability distribution of these correlation coefficients, that is the probability distribution of the null-hypothesis, is depicted in Figure 1C, red curve.

Thus, the probability to obtain the found correlation coefficient between the real TSI periodogram and the yellow histogram schematically modeling the planetary oscillations in Figure 1A (that is,  $r \approx 0.63$ ) using generic red-noise surrogate TSI records is less than 0.05%. This Monte Carlo statistical test supports the claim that the analyzed TSI record presents

dynamical spectral patterns that are better correlated to planetary harmonics than to generic red-noises that can be produced by autocorrelated signals typically generated by self evolving chaotic systems. Figure 1C also adds probability distributions of correlation coefficients between the red-noise ensemble directly with the TSI spectrum (green) and with a generic red-noise with Hurst exponent  $H = 0.95$  (blue), which is the average fractal exponent for TSI (Scafetta and West, 2005). Also these two distributions suggest that the found correlation coefficient between the planetary model and TSI,  $r \approx 0.63$ , is highly significant statistically.

### 3.2 Test #2: spectral coherence with planetary theoretical functions

The second test, using the results depicted in Figure 2, aims to determine at which planetary frequencies the strongest TSI response could be expected from hypothesized basic physical principle. Figure 2A shows the ACRIM TSI record and its periodogram as in Figure 1A. Following the arguments of Section 2 regarding the physical origins of the involved mechanisms, Figure 2 shows the MEM power spectra of the following four records for the period 1992-2013. These are calculated using JPL's HORIZONS ephemeris data downloaded from its web-interface (<http://ssd.jpl.nasa.gov/horizons.cgi>) for all solar system planets.

Panel 2B shows the energy released by tides produced from the planets on the Sun as defined in Scafetta (2012d) that uses  $m_p$  for the mass of the planet  $p$  and  $R_{pS}(t)$  for the sun-planet distance:

$$I_p(t) = \frac{3 G R_S^5}{2 Q \Delta t} \int_0^1 K(\chi) \chi^4 \rho(\chi) d\chi \cdot \int_{\theta=0}^{\pi} \int_{\phi=0}^{2\pi} \left| \sum_{p=1}^8 m_p \frac{\cos^2(\alpha_{p,t}) - \frac{1}{3}}{R_{SP}^3(t)} - m_p \frac{\cos^2(\alpha_{p,t-\Delta t}) - \frac{1}{3}}{R_{SP}^3(t-\Delta t)} \right| \sin(\theta) d\theta d\phi; \quad (3)$$

Panel 2C shows the solar z-axis component function of the planetary tidal accelerations relative to the solar equatorial reference plane, defined as

$$F_z(t) \propto \sum_{p=1}^8 \frac{m_p |z_p(t)|}{R_{SP}^4(t)}. \quad (4)$$

Panel 2D shows the speed of the Sun relative to the barycenter of the solar system as used in Scafetta (2010a) that can be directly calculated by the JPL's HORIZONS web-interface;

Panel 2E shows the jerk function (the derivative of the acceleration vector) of the Sun as defined in Scafetta (2012d)

$$\mathbf{J}_S(t) = \dot{\mathbf{a}}_S(t) = \sum_{p=1}^8 \frac{G m_p V_{SP}(t)}{R_{SP}^3(t)} \left( \frac{\mathbf{V}_{SP}(t)}{V_{SP}(t)} - 3 \frac{\mathbf{R}_{SP}(t)}{R_{SP}(t)} \right), \quad (5)$$

where  $\mathbf{V}_{SP}(t)$  is the velocity of the planet P relative to the Sun.

The four functions depicted in Panels 2B-2E stress different frequencies that may be complementary drivers for different TSI periodicities. For example, as explained above different periodicities can be activated by alternative physical mechanisms (e.g.: gravitational tides, electromagnetic interactions, geometrical asymmetry of the solar structure, etc.).

In Figure 2 we observe major frequency peaks at the periods listed in Tables 1, 2 and 3. For example, the planetary spectral peaks at the periods of about 0.2 year (cyan bar), 0.25 year (cyan bar), 0.3-0.33 year (yellow bar), 0.4 year (yellow bar), 0.65 year (yellow bar), 0.8 year (yellow bar) and 1.09 year (yellow bar) are very clear, and are found also in the TSI records (Fig. 2A). The two yellow bars in each of the spectral panels 2B-2E highlight the two most significant spectral peaks for each case.

In particular, by using these yellow bars as guides, we note the following correspondences with the TSI periodogram depicted in Figure 2A: (1) comparing Figures 2A and 2B, we find major common spectral peaks at the spring period of Venus and Jupiter (0.32 year) and other closed peaks 0.30-0.33 year, and at the spring period of Venus and Earth (0.80 year); (2) comparing Figures 2A and 2C, we find major common spectral peaks at about 0.24-0.25 year related to Mercury, at about 0.30-0.33 year related to Venus, Earth and Jupiter, and at 0.5 year related to half period of the Earth's orbit, which is strong in the solar z-axis of the tidal component because the inclination of the Earth's orbit relative to the solar equatorial plane is the largest among the planets (about  $7^\circ$ ); (3) comparing Figures 2A and 2D, we find major common spectral peaks at the synodic period of Venus and Jupiter (0.65 year) and at the synodic period of Jupiter and Earth (1.09 year); (4) comparing Figures 2A and 2E, we find major common spectral peaks at the synodic period of Venus and Mercury (0.4 year) and at the synodic period of Venus and Earth (0.65 year).

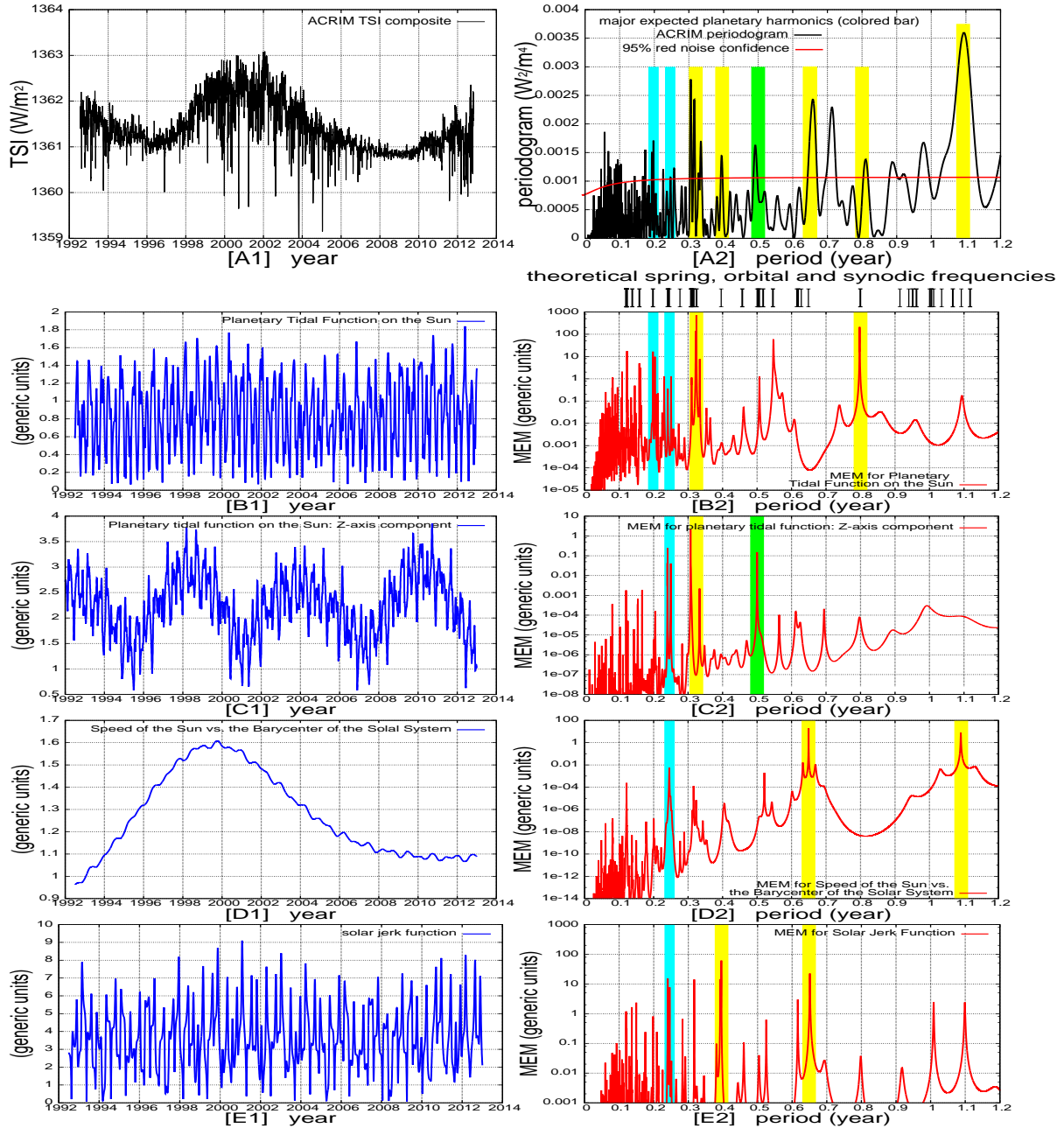


**Fig. 2** [A] Data (left) and periodogram (right) of the ACRIM TSI composite from 1992 to 2013. Data (left, blue) and MEM power spectrum analysis (right, red) of: [B] the tidal function produced by all eight planets of the solar system (from Mercury to Neptune) on the Sun as defined in Scafetta (2012d), see Eq. ??; [C] the the Z-axis component of the tidal function produced by all eight planets, see Eq. 3; [D] the speed of the Sun relative to the barycenter of the solar system as used in Scafetta (2010a) as calculated by the JPL's HORIZONS system; [E] the jerk function (the derivative of the acceleration vector) of the Sun as defined in Scafetta (2012d), see Eq. 5. The colored bars indicate the largest significant common peaks. The black small bars between panel A2 and B2 indicate all theoretical spring, orbital and synodic periods expected from the eight planets of the solar system within the analyzed period band from 0 to 1.2 year: see Tables 1 and 2. The quasi 0.7 year cycle in 2A appears to be related to the spring period of Venus beating with the synodic cycle of Earth and Jupiter (see Table 3).



The common 0.3-0.33 year harmonic cluster is made of at least three very close spectral peaks both in the TSI spectrum (Fig. 2A) and in the planetary spectrum depicted in Figure 2B-2C (see also Tables 1, 2 and 3). Other common peaks are visible, although less important. For example, the relatively strong spring harmonic between Mercury and Venus, at about 0.2 year, and the Mercury orbital harmonics at about 0.24 year are found in Figures 2A-2E. Figure 2A adds a green bar at 0.5 year that we interpret as produced by the Earth crossing the solar equator twice a year, which is also clearly visible in Figure 2C.

The black small bars between panel A2 and B2 indicate all theoretical spring, orbital and synodic periods expected from the eight planets of the solar system within the analyzed period band from 0 to 1.2 year reported in Tables 1 and 2. These results clearly suggest that the TSI record presents spectral fingerprints of multiple planetary harmonics. Thus, planetary forces likely synchronize and modulate TSI dynamics probably by means of several mechanisms.

A statistical confidence value may be estimated in the following way. The spectral interval from 0 year to 1.2 year can be divided into 20 non-overlapping bars with a width of 0.06 year each. These correspond approximately to the width of the colored bars depicted in the figures and approximately to the  $\pm 0.03$  year maximum error bar among the theoretical frequencies derived from ephemeris calculations. Figure 1A shows 11 major spectral peaks at a 95% confidence level, and at least 8 common spectral peaks are highlighted in Figure 2B-2E by the colored bars. The probability to find by random chance 8 major frequency peaks in 8 specific bars on a set of 20 available frequency range slots is about  $8!12!/20! \approx 0.001\%$ .

Note, however, that Figure 2A shows 11 spectral peaks above the 95% red-noise confidence level. The three spectral peaks that were not highlighted with colored bars are at about 0.7 year, 0.9 year and 0.96 year. These spectral peaks appear also to be present among the planetary harmonics as evident in the tables: the quasi 0.7-year cycle appears to be related to the spring period of Venus beating with the synodic cycle of Earth and Jupiter (see Table 3); the quasi 0.9-year cycle and the cycles at 0.94-1.00 years appear related to the harmonics associated with Mars (see Table 2). The probability to find by random chance 11 major frequency peaks in 11 specific bars on a set of 20 available frequency range slots is about  $9!11!/20! \approx 0.001\%$ . However, by ignoring the physical attribution of the three additional spectral peaks, which is more uncertain, it may be better to evaluate the probability to find by random chance 8 out of 11 major frequency peaks in 8 specific bars on a set of 20 available frequency range slots, which is  $(11!9!/20!) * (11!/8!/3!) \approx 0.1\%$ .

In conclusion, Figures 1 and 2 suggest a high degree of statistical coherence between the TSI periodogram and the major theoretical expected planetary frequencies.

#### 4 Interpretation of the 1.092 year TSI oscillation as an Earth-Jupiter conjunction cycle effect

In this section we propose a dynamical test to determine whether the TSI oscillations are synchronized to the planetary oscillations and whether there might be non-linear internal mechanisms causing the solar response to the external forcing vary in time. Herein, the test is limited only to the major observed oscillation of the periodogram: during the maximum of solar cycle 23,  $\sim 1.092$ -year oscillations are macroscopic and readily visible. If these oscillations are related to the Earth-Jupiter (1.092 year) synodic cycle, as the spectral analyses depicted in Figures 1 and 2 suggest, then the TSI record should present maxima in proximity of the Earth-Jupiter conjunction dates shown in Figure 3.

Figures 4A and 4B show ACRIM and PMOD (red curves) against an Earth-Jupiter (1.092 year) conjunction cycle reconstruction (black curve) for the 1998-2004 period. TSI peaks near the conjunction dates are clearly seen. The largest peak occurs near 2002 when the conjunction occurs at a minimum angular separation between Earth and Jupiter ( $0^\circ 13' 19''$ ), as expected.

Figure 4C further demonstrates the above issue showing the PMOD (blue) and ACRIM (black) records band-pass filtered to highlight their 1.0-1.2 year time-scale modulation. The two filtered curves are compared against a  $\sim 1.092$ -year harmonic function (red):

$$f(t) = g(t) \cos \left[ \frac{2\pi(t - 2002)}{1.09208} \right], \quad (6)$$

whose amplitude  $g(t)$  has been modulated on the Schwabe solar cycle. The maxima of the harmonic function well correspond to the Earth-Jupiter conjunction times as shown in Figure 3. Note that a Earth-Jupiter conjunction occurred on Jan/01/2002 and the average synodic period is 1.09208 year.

Figure 4C clearly demonstrates that the 1.0-1.2-year time-scale modulation of the TSI records is well correlated to the 1.092-year Earth-Jupiter conjunction cycle. The effect is significantly attenuated during solar minima (1995-1997 and 2007-2009) and increases during solar maxima. In particular, the figure shows the maximum of solar cycle 23 and part of the maxima of solar cycles 22 and 24.

Figure 5 compares the ACRIM and PMOD TSI composites since 1978 with two approximate empirically constructed curves comprised of the Earth-Jupiter conjunction cycle (1.09-year) as modulated by the 11-year solar cycle. The modulation

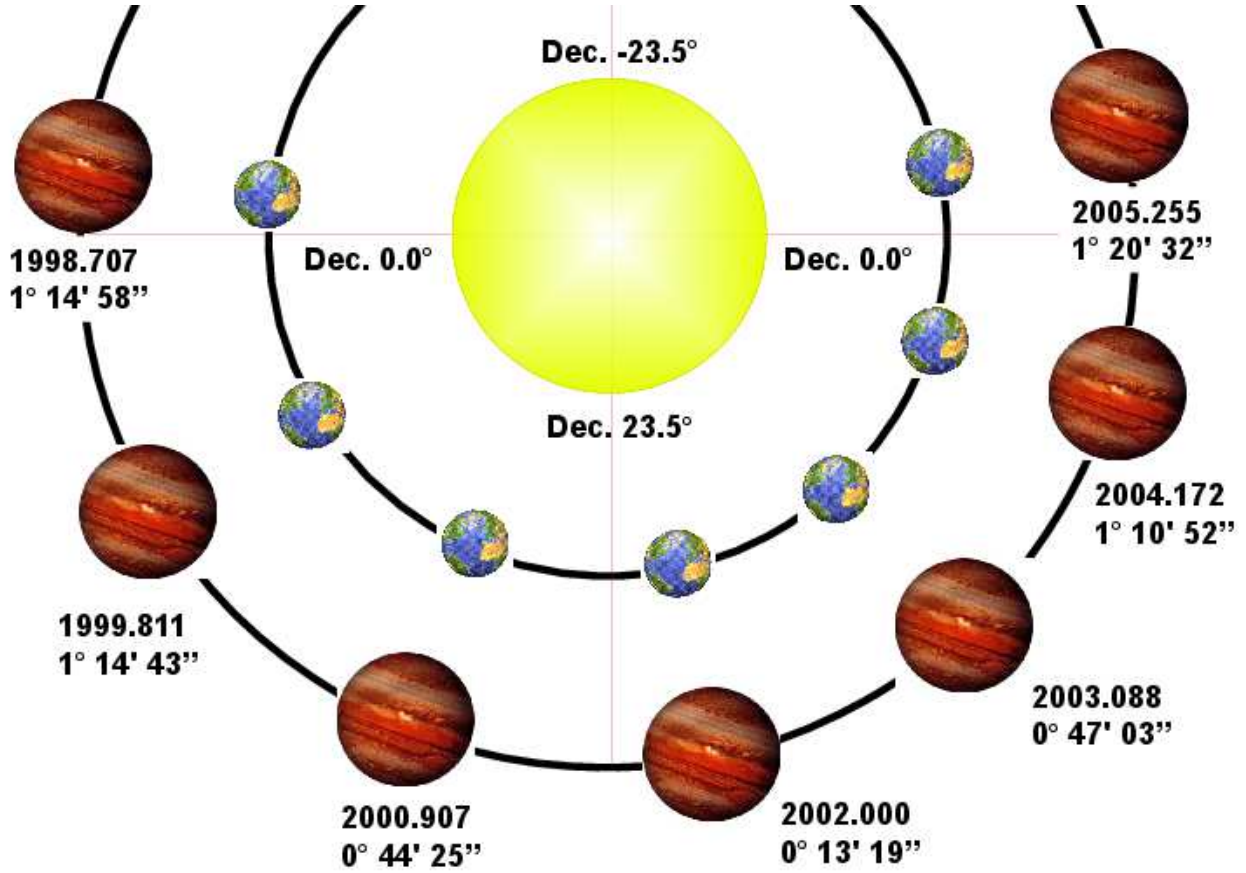


**Fig. 3** The Earth-Jupiter conjunction cycle (1.09-year) during solar cycle 23 maximum (1998-2004).

assumes that the oscillations are stronger during periods of solar maxima and are damped during solar minima. We use the following equations: for ACRIM,

$$f(t) = S_A(t) + 0.2(S_A(t) - 1360.58) \cos(2\pi(t - 2002)/1.09208); \quad (7)$$

for PMOD,

$$f(t) = S_P(t) + 0.2(S_P(t) - 1365.3) \cos(2\pi(t - 2002)/1.09208). \quad (8)$$

The blue curves are 2-year moving average smooths,  $S_A(t)$  and  $S_P(t)$ , for ACRIM and PMOD respectively. A more accurate modeling of the amplitudes of solar variation using multiple harmonics, their accurate amplitudes and their couplings is extremely complex, as ocean tidal studies would suggest (Wang et al., 2012), and are left to another study.

Using the modeled black curve as a guide, it is possible to recognize that the 1.09-year Earth-Jupiter conjunction cycle is present during the entire TSI composite period since 1978. TSI relative peaks are also found near other Earth-Jupiter conjunction dates such as in 1979, 1981, 1984, 1990, 1991, 1992, 1993, 1994, 1995, 1998, 2011 and 2012. The 1979 and 1990 peaks are less evident in PMOD, likely a result of the PMOD alteration of published Nimbus7/ERB records in 1979 and 1989 (Fröhlich, 2006; Scafetta and Willson, 2009; Scafetta et al., 2011).

The 1.09-year cycle is expected to be larger at the minimum angular separation between Earth and Jupiter. Earth's orbital inclination to the Sun's equator is  $7.16^\circ$  and Jupiter's orbital inclination is  $6.09^\circ$ . Thus, the minimum angular separation occurs when their conjunctions happen close to the solar equatorial plane. The Earth crosses the solar equator every year on Dec-08 and on Jun-07. From 1978 to 2020, Jupiter crosses the solar equator on: 1983-Jul-22, 1989-Mar-09, 1995-Jun-02, 2001-Jan-18, 2007-Apr-14, 2012-Nov-27 and 2019-Feb-23. Indeed, Figure 3 shows larger annual-scale TSI peaks in 1983, 1984, 1995, 2001, and 2002.

Finally, a TSI forecast illustration shown in Figure 5A assumes a weak solar cycle 24 that peaks in 2014 (suggested by current TSI data) with a 1.092-year modulation. The 1.09-year periodicity predicts a TSI decrease from December 2011 to May 2012 followed by a significant TSI increase from June to December 2012 since the Earth-Jupiter conjunction cycle

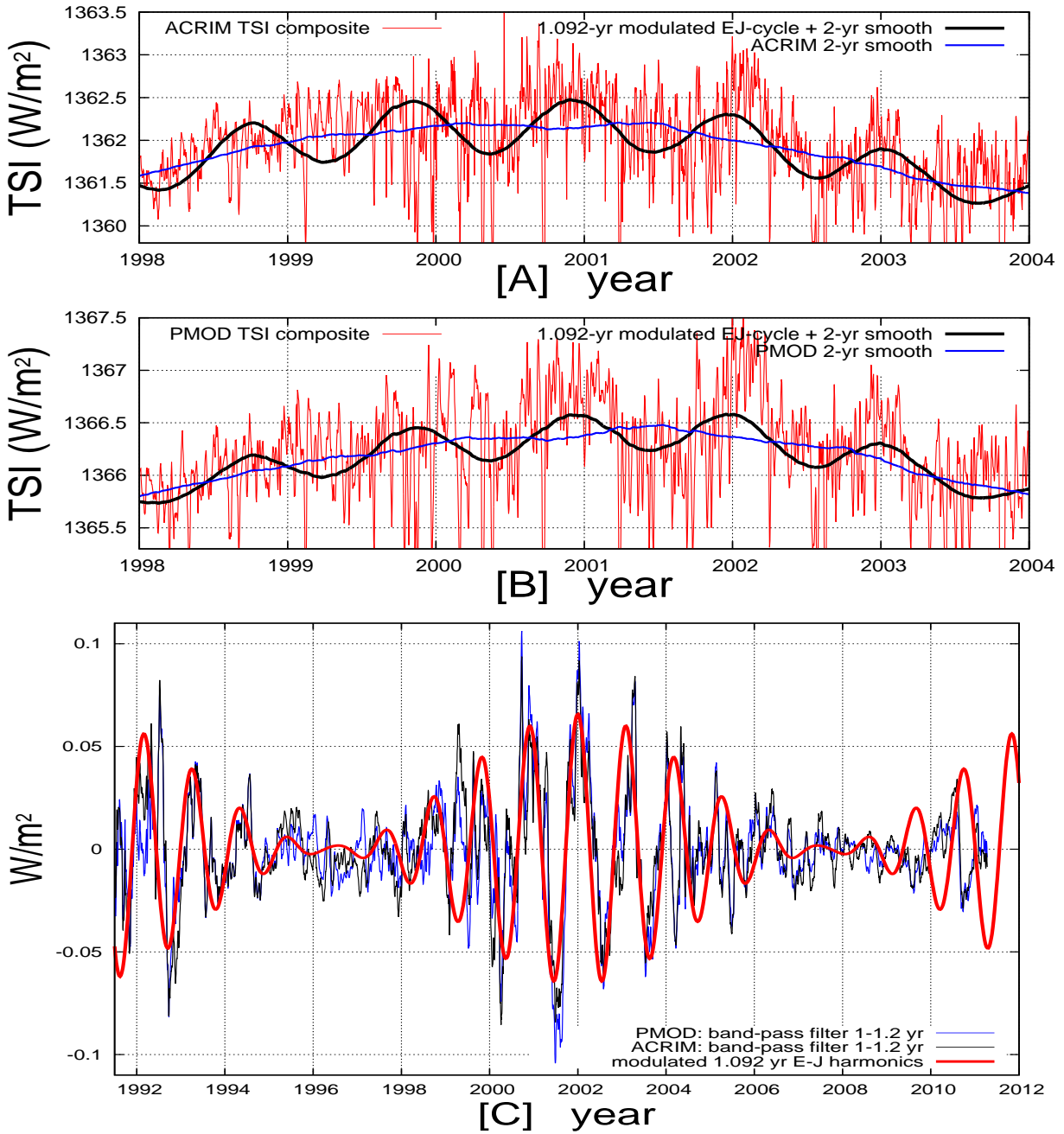


**Fig. 4** [A] ACRIM and [B] PMOD TSI composite during solar maximum 23 (1998-2004). The modeled black curve is made as in Figure 5: see Eqs. 7 and 8. [C] Moving average algorithms are used to isolate the 1-1.2 year time scale of PMOD (blue) and ACRIM (black) and compared against a 1.092-year harmonic function (red) whose amplitude is empirically modulated on the Schwabe solar cycle. The 1.092-year harmonic function is chosen in phase with the Earth-Jupiter conjunction cycle. The modeled curves are approximations used only for visualization purpose.

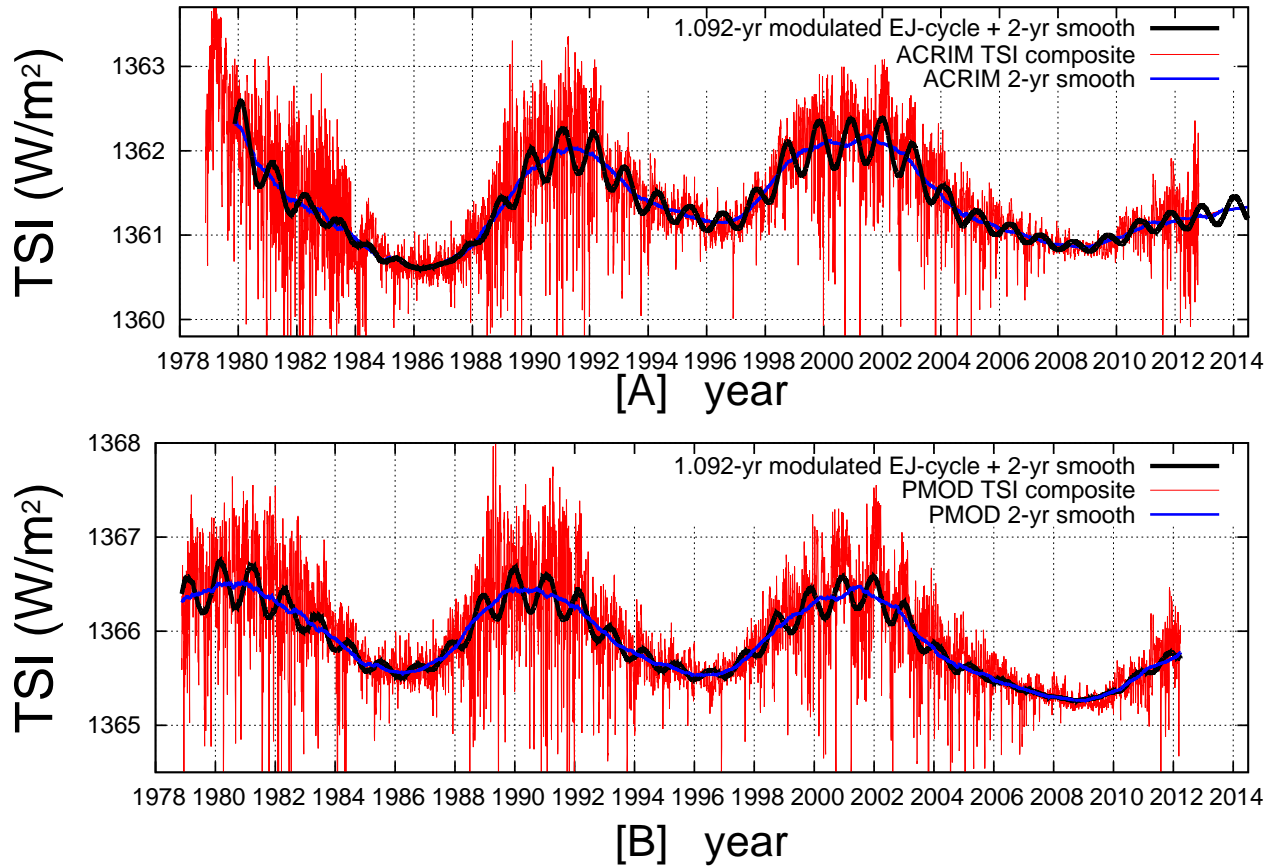


**Fig. 5** [A] ACRIM and [B] PMOD TSI satellite composites since 1978 (red). The blue curves are 2-year moving average smooth,  $S_A(t)$  and  $S_P(t)$ , for ACRIM and PMOD respectively. The black curves are empirical representations of Earth-Jupiter conjunction 1.092-year cycle modulated by the 11-year solar cycle. The modeled curves are approximations used only for visualization purpose: see Eqs. 7 and 8.

angular separation is small ( $0^\circ 38' 30''$ ). Another strong TSI peak should occur in January 2014 for a similar reason (angular separation:  $0^\circ 09' 34''$ ), followed by another maximum in February 2015. However, many other harmonics exist and interfere with each other. Therefore, the actual TSI variation patterns is expected to be more complex than suggested in the depicted simplified forecast.

## 5 Conclusions

We have investigated evidences for planetary-induced solar luminosity enhancement in the ACRIM and PMOD TSI satellite composites on monthly to annual timescales. A set of spectral peaks closely matching a set of planetary gravitational and magnetic theoretical harmonics has been found. These relatively fast cycles are primarily related to synodic and spring tidal planetary orbital combinations. The TSI power spectra present a strong peak around 0.30-0.33 year (109-121 days) that includes the spring tidal cycle of Jupiter and Venus (the strongest spring tide within the analyzed frequency band) and other closed planetary harmonics as indicated in Tables 1 and 2.

TSI records also show other clustered planetary resonances. In the 45-58 day range there are numerous Mercury spring tides and at 72 days Mercury-Venus. In the 88-91 day range there are Mercury and its synodic cycles with the Jovian planets. On the 113-120 day range there are Mercury-Earth synodic cycles and Venus-Jupiter spring tides. At 145 days there is Mercury-Venus synodic cycle. During 225-292 day periodicities there are numerous Venus related cycles. There is a major 0.5-year cycle related to the inclination of the ecliptic relative to the solar equatorial plane. A 1.092-year oscillation related to the Earth-Jupiter synodic cycle is more readily apparent during solar cycle maxima. TSI also presents spectral peaks between 0.068 year (25 days) and 0.111 year (40 days) that are related to the differential solar rotation periods (see Table 3).

Other researchers have studied the fast oscillations present in alternative solar indexes and found results compatible with ours. Rieger et al. (1984) found the quasi 25-35 days solar rotation cycles and major oscillations within 138-168 day period in energetic solar flare events, which approximately corresponds to Mercury-Venus synodic cycle. Pap et al. (1990) also

found evidences for similar oscillations; Caballero and Valdes-Galicia (2003) reported 58, 78, 89 and 115 day oscillations in cosmic rays time series; Kilcik et al. (2010) analyzed the solar flare index and reported frequency peaks close to 53, 85, 152, 248 days. More recently Tan and Cheng (2012) found evidences of planetary fast harmonics in sunspot and solar microwave records.

The 1.09-year Earth-Jupiter conjunction cycle appears to dominate in the TSI records, in particular during solar cycle maxima. Indeed, Jupiter's gravitational and magnetic interactions with the Sun are the strongest among the eight planets of the solar system. The likely explanation is that the side of the Sun facing Jupiter would be expected to be the locus of maximum interaction and cause this region to be slightly brighter causing satellite instruments to detect a slightly stronger TSI signal when the Earth crosses the Sun-Jupiter conjunction line. This coalesces with strong hot spots observed on other stars with closely orbiting giant planets (Shkolnik et al., 2003, 2005).

The amplitude dependence of the 1.09-year periodicity on the solar cycle may indicate that in addition to gravitational tidal interaction (Wolff and Patrone, 2010; Scafetta, 2012d), there may also exist a solar dynamo amplification mechanism that varies with the Schwabe solar cycle. There may also exist an enhancement related to the interplanetary magnetic field structure linking the planets along the Parker spiral of the stellar wind (Kopp et al., 2011; Gurdemir et al., 2012).

The harmonics present in the variability of satellite TSI satellite observations indicate that planetary forcings are likely modulating solar activity and that both magnetic and gravitational coupling are involved. Future research will better address the nature of these couplings, which could provide better forecast capability for solar activity and climate change. It has been shown in recent studies that both solar and climate records present strong signatures of planetary cycles at decadal, secular and millennial time scales (Scafetta, 2010a, 2012a,b,c,d; Scafetta and Willson, 2013; Scafetta et al., 2013).

#### Acknowledgment

The National Aeronautics and Space Administration supported Dr. Willson under contracts NNG004HZ42C at Columbia University, Subcontracts 1345042 and 1405003 at the Jet Propulsion Laboratory.

#### References

- Abreu, J. A., Beer, J., Ferriz-Mas, A., McCracken, K. G., Steinhilber, F., 2012. *A&A*, 548A, 88A.
- Baliunas, S. L. et al., 1995. *Apj* 438, 269.
- Ball, W. T., Unruh, Y. C., Krivova, N. A., Solanki, S., Wenzler, T., Mortlock, D. J., Jaffe, A. H., 2012. *A&A*, 541, A27.
- Bendandi, R., 1931. *Un Principio Fondamentale dell'Universo*. S.T.E. Faenza, Italy.
- Bigg, E. K., 1967. *Astron. J.*, 72, 463.
- Bond, G., et al., 2001. *Science*, 294, 2130.
- Brown, E. W., 1900. *MNRAS*, 60, 599.
- Caballero, R., Valdes-Galicia, J. F., 2003. *Solar Phys.* 213, 413.
- Callebaut, D.K., de Jager, C., Duhau, S., 2012. *J. Atmos. Sol.-Terr. Phys.*, 80, 73.
- Charvátová, I., Střeščík, J., 1991. *J. Atmos. Sol.-Terr. Phys.*, 53, 1019.
- Chylek, P., et al., 2012. *Geophys. Res. Lett.*, 39, L09705.
- Cionco, R. G., Compagnucci, R. H., 2012. *Advances in Space Research* 50, 1434.
- Courtillot, V., Le Mouel, J. L., Mayaud, P. N., 1977. *J. Geophys. Res.*, 82, 2641.
- Cuntz M., Saar, S. H., and Musielak, Z. E., 2000. *APJ*, 533, L151.
- Doodson, A.T., 1921. *Proceedings of the Royal Society of London Series A* 100 (704), 305–329.
- Duric, N., 2004. *Advanced Astrophysics*, (Cambridge University Press).
- Fairbridge, R. W., Shirley, J. H., 1987. *Sol. Phys.*, 10, 191.
- Frick, P., Galyagin, D., Hoyt, D V, Nesme-Ribes, E., Schatten, K.H., Sokoloff, D., Zakharov, V., 1997. *A&A*, 328, 670.
- Fröhlich, C., 2006. *Space Sci. Rev.*, 125, 53.
- Ghil, M. et al., 2002. *Rev. Geophys.* 40, 3.1-3.41.
- Gurdemir, L., Redfield, S., Cuntz, M., 2012. *PASA Austr. J. of Chem.* 29, 141.
- Hung, C.-C., 2007. *NASA/TM-2007-214817*.
- Jiang, J., Chatterjee, P., Choudhuri, A.R., 2007. *Monthly Notices of the Royal Astronomical Society* 381, 1527.
- Jose, P.D., 1965. *Astron. J.*, 70, 193.
- Juckett, D.A., 2000. *Sol. Phys.* 191, 201.
- Juckett, D.A., 2003. *A&A* 399, 731.
- Kelvin (Lord Thomson, W.), 1881. *Proceedings of the Institution of Civil Engineers* 65, 3.
- Kilcik, A., Ozguc, A., Rozelot, J.P., Atas, T. 2010. *Solar Phys.*, 264, 255.

- Kopp, A., Schilp, S., Preusse, S., 2011. *ApJ*, 729, 116.
- Landscheidt, T., 1999. *Sol. Phys.*, 189, 415.
- Leal-Silva M. C., Velasco Herrera, V. M., 2012. *J. Atmos. Sol.-Terr. Phys.* 89, 98.
- Luby, W.A., 1948. *Popular Astronomy* 56, 252.
- Ogurtsov, M. G., Nagovitsyn, Y. A., Kocharov, G. E., Jungner, H., 2002. *Solar Phys.* 211, 371.
- Pap, J., Tobiska, W.K., Bouwer, S.D., 1990. *Solar Phys* 129, 165.
- Press, W.H., Teukolsky, S.A., Vetterling, W.T., Flannery, B.P., 1997. *Numerical recipes in C*. (Cambridge University Press).
- Poppenhaeger, K., Schmitt J. H. M. M., 2011. *ApJ* 735, 59.
- Pikovskiy, A., Roseblum, M., Kurths, J., 2001. *Synchronization: A Universal Concept in Nonlinear Sciences*. (Cambridge University Press).
- Qian, W.H., Lu, B., 2010. *Chinese Sci. Bull.* 55, 4052.
- Rieger, E., Kanbach, G., Reppin, C., Share, G. H., Forrest, D. J., Chupp, E. L., 1984. *Nature* 312, 623.
- Scafetta, N., West, B. J., 2003. *Physical Review Letters* 90, 248701.
- Scafetta, N., Grigolini, P., Imholt, T., Roberts, J. A., West, B. J., 2004. *Physical Review E* 69, 026303.
- Scafetta, N., West, B.J., 2005. *Complexity* 10, 51-56.
- Scafetta, N., Willson, R. C., 2009. *Geophys. Res. Lett.*, 36, L05701.
- Scafetta, N., 2010a. *J. Atmos. Sol.-Terr. Phys.* 72, 951.
- Scafetta, N., 2010b. Abstract GC21B-0868 *Poster*, presented at 2010 Fall Meeting, AGU, San Francisco, Calif., 13-17 Dec.
- Scafetta, N., 2011. In *Evidence-Based Climate Science*, (edited by Easterbrook D., Elsevier), 12, 289.
- Scafetta, N., 2012a. *J. Atmos. Sol.-Terr. Phys.* 74, 145.
- Scafetta, N., 2012b. *J. Atmos. Sol.-Terr. Phys.*, 80, 124.
- Scafetta, N., 2012c. *J. Atmos. Sol.-Terr. Phys.*, 80, 296.
- Scafetta, N., 2012d. *J. Atmos. Sol.-Terr. Phys.*, 81-82, 27.
- Scafetta, N., Willson, R. C., 2013. *Planetary and Space Science* 78, 38.
- Scafetta, N., O. Humlum, J.-E. Solheim, and K. Stordahl, 2013. *J. Atmos. Sol.-Terr. Phys.* DOI: 10.1016/j.jastp.2013.03.007
- Scharf, C. A., 2010. *ApJ*, 722, 1547.
- Sharp, G.J., 2013. *International Journal of Astronomy and Astrophysics* 3(3), in press. <http://arxiv.org/abs/1005.5303>
- Shkolnik, E., Walker, G. A. H., Bohlender D. A., 2003. *ApJ*, 597, 1092.
- Shkolnik, E., Walker, G. A. H., Bohlender, D. A., Gu P.-G., Kurster, M., 2005. *ApJ*, 622, 1075.
- Shravan, M. H., Thomas, L. D. Jr., Katepalli, R. S., 2012. *PNAS* 109, 11928.
- Smythe, C. M., Eddy, J. A., 1977. *Nature* 266, 434.
- Steinhilber, et al., 2012. *PNAS* 109, 5967.
- Sturrock, P. A., Caldwell, D. O., Scargle, J. D., 2006. *Astroparticle Physics* 26, 174.
- Tan B., 2011. *Astrophys Space Sci.* 332, 65.
- Tan B., Cheng Z., 2012. *Astrophys Space Sci.* 343, 511.
- Tobias, S. M., 2002. *PTRS A*, 360, 2741.
- Wang, Z., Wu, D., Song, X., Chen, X., Nicholls, S., 2012. *J. Geophys. Res.*, 117, D07102.
- Willson, R. C., Gulkis, S., Janssen, M., Hudson, H. S., Chapman, G. A., 1981, *Science* 211, 700.
- Willson, R. C., Hudson, H. S., Fröhlich, C., Brusa, R. W., 1986. *Science* 234, 1114.
- Willson, R. C., Hudson, H. S., 1991. *Nature* 351, 42.
- Willson R. C., 1997. *Science*, 277, 1963.
- Willson, R. C., Mordvinov, A. V., 2003. *Geophys. Res. Lett.* 30, 1199.
- Wilson, I. R. G., Carter, B. D., Waite, I. A., 2008. *Publications of the Astronomical Society of Australia* 25, 85.
- Wolf, R., 1859. *MNRAS* 19, 85.
- Wolff, C. L., Patrone, P. N., 2010. *Sol. Phys.* 266, 227.
- Wood, R.M., Wood, K.D., 1965. *Nature* 208, 129.
- Wright, J. T., et al., 2008. *ApJ*, 683, L63.

Cycle	Type	P (day)	P (year)	min (year)	max (year)	strength
Me	1/2 orbital	44 ± 0	0.120 ± 0.000	0.120	0.121	u
Me – Ju	spring	45 ± 9	0.123 ± 0.024	0.090	0.156	u/w
Me – Ea	spring	58 ± 10	0.159 ± 0.027	0.117	0.189	u/w
Me – Ve	spring	72 ± 8	0.198 ± 0.021	0.156	0.219	u/w
Me	orbital	88 ± 0	0.241 ± 0.000	0.241	0.241	u
Me – Ju	synodic	90 ± 1	0.246 ± 0.002	0.243	0.250	u
Ea	1/4 orbital	91 ± 3	0.250 ± 0.000	0.250	0.250	w
Ve	1/2 orbital	112.5 ± 0	0.307 ± 0.000	0.307	0.308	w
Me – Ea	synodic	116 ± 9	0.317 ± 0.024	0.290	0.354	u/w
Ve – Ju	spring	118 ± 1	0.324 ± 0.003	0.319	0.328	u
Ea	1/3 orbital	121 ± 7	0.333 ± 0.000	0.333	0.333	w
Me – Ve	synodic	145 ± 12	0.396 ± 0.033	0.342	0.433	u/w
Ea	1/2 orbital	182 ± 0	0.500 ± 0.000	0.500	0.500	u
Ea – Ju	spring	199 ± 3	0.546 ± 0.010	0.531	0.562	w
Ve	orbital	225 ± 0	0.615 ± 0.000	0.615	0.615	w
Ve – Ju	synodic	237 ± 1	0.649 ± 0.004	0.642	0.654	u
Ve – Ea	spring	292 ± 3	0.799 ± 0.008	0.786	0.810	u/w
Ea	orbital	365.25 ± 0	1.000 ± 0.000	1.000	1.000	w
Ea – Ju	synodic	399 ± 3	1.092 ± 0.009	1.082	1.104	u/s
Ea – Ve	synodic	584 ± 6	1.599 ± 0.016	1.572	1.620	u

**Table 1** List of the major theoretical expected harmonics associated with planetary orbits within 1.2 year period.  $P$  is the period of the harmonic; see also Eq. 1. Mercury (Me), Venus (Ve), Earth (Ea), Jupiter (Ju). The variability ranges are based on ephemeris calculations. The strength (last column) is qualitatively estimated as: uncertain/strong (u/s); weak (w); uncertain (u); uncertain/weak (u/w).

Cycle	Type	P (year)	Type	P (year)
Me – Ne	spring	0.1206	synodic	0.2413
Me – Ur	spring	0.1208	synodic	0.2416
Me – Sa	spring	0.1215	synodic	0.2429
Me – Ma	spring	0.1382	synodic	0.2763
Ve – Ne	spring	0.3088	synodic	0.6175
Ve – Ur	spring	0.3099	synodic	0.6197
Ve – Sa	spring	0.3142	synodic	0.6283
Ve – Ma	spring	0.4571	synodic	0.9142
Ea – Ne	spring	0.5031	synodic	1.006
Ea – Ur	spring	0.5060	synodic	1.0121
Ea – Sa	spring	0.5176	synodic	1.0352
Ea – Ma	spring	1.0676	synodic	2.1352
Ma	1/2 orbital	0.9405	orbital	1.8809
Ma – Ne	spring	0.9514	synodic	1.9028
Ma – Ur	spring	0.9621	synodic	1.9241
Ma – Sa	spring	1.0047	synodic	2.0094
Ma – Ju	spring	1.1178	synodic	2.2355
Ju	1/2 orbital	5.9289	orbital	11.858
Ju – Ne	spring	6.3917	synodic	12.783
Ju – Ur	spring	6.9067	synodic	13.813
Ju – Sa	spring	9.9310	synodic	19.862
Sa	1/2 orbital	14.712	orbital	29.424
Sa – Ne	spring	17.935	synodic	35.870
Sa – Ur	spring	22.680	synodic	45.360
Ur	1/2 orbital	41.874	orbital	83.748
Ur – Ne	spring	85.723	synodic	171.45
Ne	1/2 orbital	81.862	orbital	163.72

**Table 2** List of additional average theoretical expected harmonics associated with planetary orbits: Mercury (Me), Venus (Ve), Earth (Ea), Mars (Ma), Jupiter (Ju), Saturn (Sa), Uranus (Ur), Neptune (Ne). See Eq. 1.

Cycle	Type	P (year)	Type	P (year)
Sun	equ-rot	0.068	pol-rot	0.094
Sun – Ju	equ-rot	0.068	pol-rot	0.095
Sun – Ea	equ-rot	0.073	pol-rot	0.104
Sun – Ve	equ-rot	0.076	pol-rot	0.111
Sun – Me	equ-rot	0.095	pol-rot	0.154
Me – (Ju – Sa)	spring	0.122	synodic	0.244
Me – (Ea – Ju)	spring	0.155	synodic	0.309
Ve – (Ju – Sa)	spring	0.317	synodic	0.635
Ea – (Ju – Sa)	spring	0.527	synodic	1.053
Ve – (Ea – Ju)	spring	0.704	synodic	1.408

**Table 3** Partial list of additional theoretical harmonics. First rows: solar equatorial (equ-) and polar (pol-) rotation cycles relative to the fixed stars and to the four major tidal planets calculated using Eq. 1. Other rows report the spring and synodic periods of Mercury, Venus and Earth relative to the synodic periods of Jupiter and Saturn, and Earth and Jupiter. The latter periods are calculated using Eq. 2.